

**Coordination chemistry of lanthanides in AOT-CMPO solvent extraction system: UV-Vis and XAFS studies**

| | |
|-------------------------------|--|
| Journal: | <i>Dalton Transactions</i> |
| Manuscript ID | DT-ART-07-2018-002957.R1 |
| Article Type: | Paper |
| Date Submitted by the Author: | 11-Sep-2018 |
| Complete List of Authors: | Moon, Jisue; University of California Irvine, Chemical Engineering and Materials Science Nilsson, Mikael; University of California Irvine, Chemical Engineering and Materials Science; University of California Irvine, Chemistry |
| | |



Journal Name

ARTICLE

Coordination chemistry of lanthanides in AOT-CMPO solvent extraction system: UV-Vis and XAFS studies

Received 00th January 20xx,
Accepted 00th January 20xx

Jisue Moon^a and Mikael Nilsson^{*a,b}

DOI: 10.1039/x0xx00000x

www.rsc.org/

The extractability and coordination chemistry for lanthanides in a binary extraction system containing Aerosol OT (AOT) and a phosphine oxide (CMPO) has been investigated by means of UV-Vis and X-ray Absorption Fine Structure (XAFS) techniques over a range of extractant concentrations. In addition to Fourier transform EXAFS analysis, the application of wavelet transforms (WT) to the Fourier transform was adapted to Ho L-III edge to provide a better contrast between the heavier and lighter backscattering atoms at higher coordination shells in the mixed extractant system. Through the variation of the ratio of AOT and CMPO and the acid concentration of aqueous phase, a synergistic effect appeared at a 1:1 ratio of AOT and CMPO using moderate acid concentration (0.5 M HNO₃). It was also found that CMPO itself is directly coordinated with the metal ions by forming the bond with P=O and C=O, while AOT extract the lanthanide as a hydrated form through reverse micelle formation. However, the complex of CMPO (C=O-M and P=O-M) to metal gets weaker as it is mixed with AOT. Our results indicate that complexation from the CMPO is aiding the control of water extraction through reverse micelles from AOT, which results in the cooperative effect of certain mixtures of AOT-CMPO. The information from this coordination environment offers insight into the role of reverse micelle formation in mixed-extractant solvent extraction system.

Introduction

Solvent extraction has been applied successfully in various fields including the pharmaceutical industry, the production of precious metals and rare-earth elements, and in the chemical treatment of used nuclear fuel¹⁻¹¹. In the practice of solvent extraction for chemical separation, amphiphilic extractants are used in a biphasic solution system to remove the target solutes, e.g. metal ions, from an aqueous phase. The targeted solute is bound selectively by the extractant or incorporated in a reverse micelle in the organic phase^{12,13}. The effects of the combination of multiple extractants in a system have been studied extensively due to the synergistic enhancement of certain extractants. For example, Aerosol OT (AOT) has been used in combination with other extractants in systems that display synergistic extraction, such as carbamoylmethylene phosphine oxide (CMPO)¹⁴, bulky amides¹⁵ or N,N',N',N'-tetra(n-octyl)diglycolamide (TODGA)¹⁶. Those additional extractants by themselves are not surface active enough to create extensive reverse micelle formation. The improvement observed when combining it with AOT may be due to the formation of reverse micelles and, while not well understood, could be very important.

In the present study, we investigate how a combination of

AOT and CMPO (Figure 1) in an extraction system for metal ions affects the solute extractability and the phase stability with respect to coordination chemistry. The goal of this study is to improve the understanding of the extraction mechanism for extractants in a synergistic system. Probing the coordination environment around the metal ion and investigating the extracted complex on a molecular level could allow for establishing new extractants with improved properties. Holmium (Ho) and erbium (Er) were chosen as a target metals due to their spectroscopic properties that include hypersensitive bands responsive to the coordination and geometry of the surroundings. Water, metal ion and nitric acid extraction were carefully monitored as a function of AOT to neutral extractant concentration ratio. The complexation state of extracted species with AOT and CMPO was investigated by spectroscopic analysis such as UV-Vis spectroscopy¹⁷⁻¹⁹ and X-ray Absorption Spectroscopy (XAS).

For certain lanthanides, the electron transitions are hypersensitive to the symmetry and electronic field strength of the metal such as ⁵I₈ → ⁵G₆ transition for Ho and ⁴I_{15/2} → ²H_{12/2} transition for Er. Since the mechanism of each extractant, AOT and CMPO, are different, the electron transition of the extracted lanthanide will help to understand if and how the lanthanide environment changes during the extraction. In addition to the UV-Vis study, we applied X-ray Absorption spectroscopy (XAS) as a technique to better understand the coordination chemistry around the metal ions. The Fourier transform of extended X-ray absorption fine structure (EXAFS) enables a first qualitative estimate of how many atoms are

^a Department of Chemical engineering and Materials Science, University of California, Irvine, 916 Engineering Tower, Irvine, CA 92697-2575, USA

^b Department of Chemistry, University of California Irvine, 1102 Natural Science 2, Irvine, CA 92697-2025, USA. Email: nilssonm@uci.edu

present in each coordination shell at certain distance surrounding the absorbing atom. This is done by analyzing the spectrum in either *k* or *R* space through Fourier transform²⁰. XAS has been used to provide local structure of molecules

UV-vis and XAFS to understand the mixed extractant system and the role of each extractant.

Experimental Section

Material

Aqueous solutions of 0.01 M of holmium and erbium were prepared by first dissolving holmium oxide (99.999%) and erbium oxide (99.999%) provided by Michigan Metals & Manufacturing, in nitric acid to prepare a stock holmium or erbium nitrate solution that could then be diluted to appropriate concentration. These solutions were subsequently standardized for Ho^{3+} and Er^{3+} concentrations, acidity (H^+ concentration), and excess nitrate concentration by a combination of neutron activation analysis, UV-Vis, potentiometric titration, and ion chromatography. The lanthanide concentration was determined by taking samples of the prepared solutions along with samples of various dilution of ICP-MS standard solutions of each lanthanide (1,000 ppm Ln(III) in 2% HNO_3 , Inorganic Ventures). For the neutron activation, the solutions and standards were irradiated in the UC Irvine TRIGA[®] reactor to create radioactive isotopes of holmium (^{166}Ho) by the n,γ reaction. Post irradiation the samples were analysed using a high purity germanium detector (Canberra, 40% relative efficiency, 1.8 keV FWHM at 1.332 MeV) measuring the gamma energy of ^{166}Ho . The activity of each sample was corrected for decay time. The activity was related to known concentration for the standard samples and this correlation was used to calculate the concentration of the unknown solutions. UV-Vis spectroscopy was carried out using an Olis upgraded Cary 14 UV-vis-NIR spectrometer with a jacketed cell held at 20 °C to standardize the erbium solutions. The solutions of ICP-MS standards were measured and a calibration curve of absorption vs. concentration was prepared and used to calculate the concentration in the unknown samples. The potentiometric titrations were carried out by titrating the lanthanide solutions with standardized sodium hydroxide using a Metrohm 836 Titrand auto-titrator. The results were corrected for the known lanthanide concentration to find the acid concentration. Finally, the nitrate concentration of each sample was determined by using a Metrohm 850 ion chromatograph, supplied by Metrohm USA Inc. through the UC Irvine Metrohm Lab. Concentrated nitric acid (15.8 M) was supplied by Marcon Fine Chemicals. Water used to dilute the concentrated solutions was obtained from an in-house source of ultrapure (18.2 M Ω -cm) water. Sodium nitrate was obtained from Fischer Scientific and was filtered and recrystallized before use. Sodium docusate (AOT) anhydrous was obtained from Fisher Scientific to >99% purity. CMPO was obtained at 96% purity from Marshallton. Organic solutions containing different concentration of AOT and CMPO were prepared by dissolving the reagents in heptane (HPLC grade, >99.0%) obtained from OmniSolv. The organic chemicals were all used without any further purification.

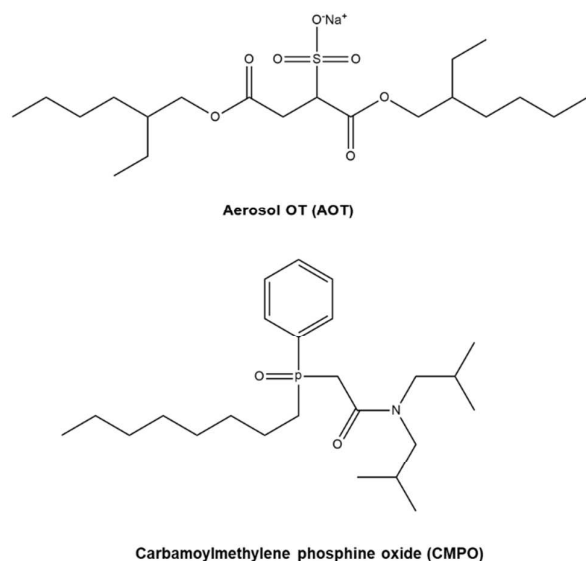


Figure 1. Structures of Aerosol OT (AOT) and carbamoylmethylene phosphine oxide (CMPO) employed in the present study.

predominantly in inorganic systems. The ability to excite electrons in selected atoms permits for the distinguishing of metal-ligand coordination details at specific position in molecules. For example, the coordination chemistry of selected actinides and lanthanides in nitrate and chloride solutions has been studied to understand the aqueous phase speciation of the metal ions^{21,22}. Furthermore, this technique has been used to study the coordination environment of metals extracted in the organic phase by various ligands, including oxygen coordinating ligands like CMPO²³ and TODGA²⁴ as well as nitrogen coordinating ligands²⁵. Finally, this technique has been used successfully in past studies of synergistic extraction systems to obtain details regarding the role of each extractant^{26,27,28}. In addition to XAFS analysis, wavelet-based XAFS analysis is a dedicated method to elucidate the elemental feature and spatial location of the neighbors surrounding the X-ray absorber^{29,30}. Especially in solvent extraction system, the extraction conducted with soft donor or mixed donor systems will result in complexes which have similar bond length between the targeted metal ion and the different donor groups. To better understand these systems, wavelet transform (WT) of Fourier transform was adapted for discriminating the backscattering atoms by their elemental nature. The WT can resolve the *k* dependence of the absorption signals and therefore gives better contrast between heavier and lighter backscattering atoms, even if they are at the same distance from the central atom^{30,31}. The aim of this work is to investigate the coordination chemistry by means of

Solvent extraction

XAFS investigations were performed at beamline 10-BM-B of the Advanced Photon Source at Argonne National

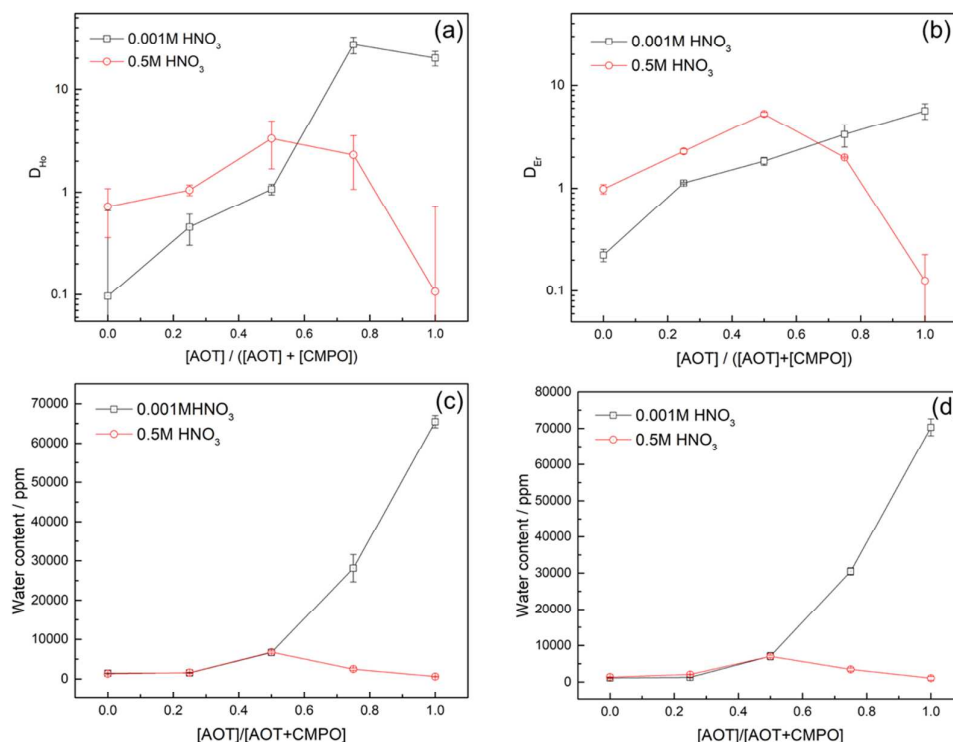


Figure 2. Distribution ratio of holmium (a) and erbium (b) and concentration of water in the organic phase from holmium extraction (c), and erbium extraction (d) as a function of $[AOT]/[AOT+CMPO]$ mole ratio after contact with 0.001 M HNO_3 (black) or 0.5 M HNO_3 (red) aqueous phase containing 0.01 M Ho^{3+} or 0.01 M Er^{3+} . The error bars represent standard deviations from triplicate measurement.

Solvent extraction experiments using AOT and CMPO in heptane were performed by contacting equal volumes of the organic and aqueous phase for 5 min using a vortex mixer followed by centrifugation at 3000 rpm for 3 min. After centrifugation, aliquots of each phase were taken for analysis. The distribution ratios of Ho were determined by neutron activation analysis using the UC Irvine TRIGA[®] reactor as described above. The distribution ratio of erbium was measured by UV-Vis analysis from the difference of the aqueous phase concentration before and after extraction. UV-vis spectra of the organic phases were collected on the Olis upgraded Cary 14 UV-vis-NIR spectrometer. The organic phase spectra were collected after extraction with different extractant concentrations. The water concentration in the organic phase was determined by Karl Fisher titrations using a Metrohm KF Titrando with each sample measured in duplicate. The Karl-Fisher measurements were checked for accuracy using standardized solutions of 1 mg water per 1 g solution, HYDRANAL[®] Water Standard 1.0 obtained from Fisher Scientific.

XAFS Measurement

Laboratory³². Spectra were collected at the holmium L-III edge (8071 eV) and Erbium L-III edge (8358 eV) in fluorescence mode with a Hitachi Vortex-ME4 four element silicon drift fluorescence detector. For all samples, data sets were collected until adequate signal to noise was obtained, in all instances between 3 to 10 scans. The X-ray white beam was monochromatized by a Si (1 1 1) monochromator and detuned 50% to reduce the contribution of higher-order harmonics. All samples were collected at room temperature.

Data were processed with the Athena and Artemis programs of the IFEFFIT package³³. Spectra were averaged in $\mu(E)$ data, which was calibrated to the literature E_0 value for each elements edge. Background removal was achieved by spline fitting. EXAFS data were extracted above the threshold energy, E_0 . The conventional metrical analysis of the Ho and Er $k^3\chi(k)$ EXAFS was performed. Fit windows in k space were determined based on the lowest quality data collected and for all data sets were from 1 to 9 \AA^{-1} . In all fits, the amplitude reduction factor (S_0^2) was performed with a fixed scale factor as 0.9. Independent structural parameters determined by the fits included the change in the scattering half path length (ΔR_i) and the relative mean square displacement of the scattering element (σ_i^2). For each fit, the number of variables was not

permitted to exceed 2/3 the number of independent points, in keeping with the Nyquist criterion.

Wavelet transform EXAFS

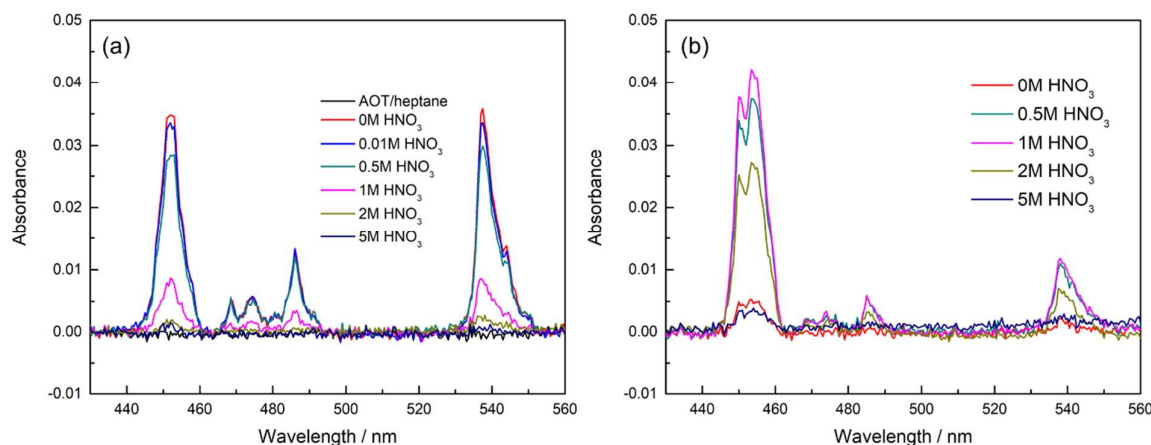


Figure 3. UV-vis absorption spectra of organic phases for the acid concentration dependency for holmium extraction with (a) 0.01 M AOT in heptane and (b) 0.01 M CMPO in heptane. Extraction conducted with 0.01 M $\text{Ho}(\text{NO}_3)_3$ dissolved in nitric acid of different concentration.

A qualitative analysis of the property of the backscattering atoms in the higher coordination shells was conducted using the wavelet transform (WT) method implemented in the EvAX code³⁴. These WT results are typically visualized as contour plots in three dimensions including the wave vector (k), the interatomic distance uncorrected for phase shift (R) and the WT modulus. Contributions from different back-scattering atoms at specific regions in k and R space are visualized in the plots as ridges and the location of the ridges helps to differentiate between light and heavy backscattering atoms³⁰.

Result and Discussion

Extraction study

Solvent extraction experiments were performed at varying AOT ratio ($[\text{AOT}]/([\text{AOT}]+[\text{CMPO}]) = 1, 0.75, 0.5, 0.25, 0$) keeping total extractant concentration (AOT + CMPO) at 0.05 M in the organic phase and contacting with an aqueous phase of different nitric acid concentration with 0.01 M Ho^{3+} or Er^{3+} . Figure 2 (a) and (b) shows the variation of distribution ratio of Ho^{3+} and Er^{3+} , defined as the ratio of the concentration of the metal between the organic and aqueous phase. For the extraction from low acid concentrations, an increasing trend for both holmium and erbium is observed although erbium shows lower distribution ratios at high AOT concentration compared to holmium. When the acid concentration of the aqueous phase increase, a nonlinear trend for both holmium and erbium was observed. At an AOT ratio of 0.5 when the higher acid concentration was used, the distribution ratio of holmium and erbium increased from 0.7 to 2 and from 1 to 4, respectively. This suggest that the cooperative effect of CMPO is possibly due to the increase of extractability of CMPO at higher acid concentration. CMPO is well known to extract

trivalent actinides, as well as lanthanides, with improved extraction at moderate HNO_3 concentration³⁵. For the experiments at high acid concentration, the distribution ratio drastically decreases at higher AOT concentrations, which can be explained by the deformation of AOT at higher acid

concentration⁷ and the concentration of CMPO not being enough to extract additional lanthanides from the aqueous phase. Furthermore, at elevated nitric acid concentration CMPO is known to extract HNO_3 which may compete with the metal uptake^{36,37}. The fact that the distribution ratios, in the high acid case, for an AOT ratio of 0 is lower compared to the AOT ratio of 0.5 suggest that there is a synergistic effect. If there was no synergistic effect the solvent using 0.05 M CMPO alone should provide the highest extraction at high acid.

In addition to the distribution ratio, the water content of the organic phase at each AOT ratio was analyzed and is shown in figure 2 (c), (d). A linear trend for Ho^{3+} and Er^{3+} were observed for low acid concentration, but a non-linear trend is observed for the high acid concentration. While the water content trend is similar to the trend of the metal distribution ratio at high nitric acid concentration, the differences in water content between high and low acid case at AOT ratios of 0.25 and 0.5 were very small. This suggests that the amount of reverse micelle formed is similar between low and high acid concentration, at these AOT ratios. Due to the amphiphilic property of AOT, it can dissolve in both the aqueous and the organic phase and cause a phase change from micelle to emulsion phase if enough water is extracted into the organic phase³⁸. From our previous study³⁹, the emulsion phase of the organic phase occurred at lower AOT concentration, less than 0.02 M AOT, but the emulsion in the aqueous phase formed when AOT was added in a concentration above 0.02 M. However, this phenomenon did not occur for the mixed AOT-CMPO system and both phases were clear.

UV-Vis absorption spectroscopy

UV-vis spectra of organic phases after extraction of metal ions from different aqueous acid concentration were collected at the wavelengths covering the hypersensitive absorption band. The holmium ion has a hypersensitive band centered

around 450 nm, related to the $^5I_8 \rightarrow ^5G_6$ transition. Depending on the coordination number and environment around the lanthanide atom, the peak shape and the intensity change drastically^{18,40}.

CMPO extraction, as expected. This high intensity around 450 nm for CMPO extraction is remarkable, indicating very intense hypersensitive transition compared with the same transition in AOT extraction. This can be explained by differences in the coordination

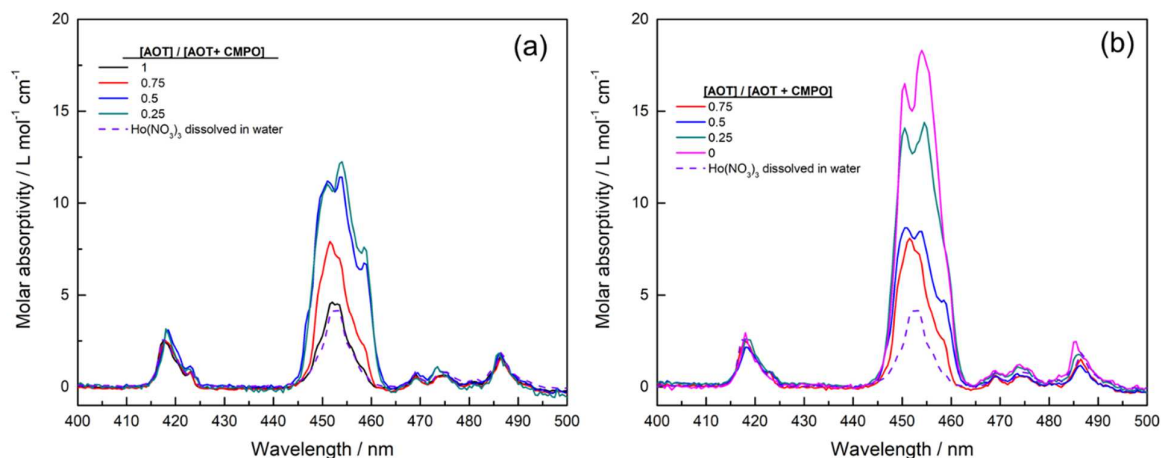


Figure 4. UV-vis absorption spectra of the organic phase after extraction varying extractants concentrations (legend shows the ratio of [AOT]/([AOT+CMPO])) with the aqueous phase including Ho³⁺ in (a) 0.001 M HNO₃ and (b) 0.5 M HNO₃.

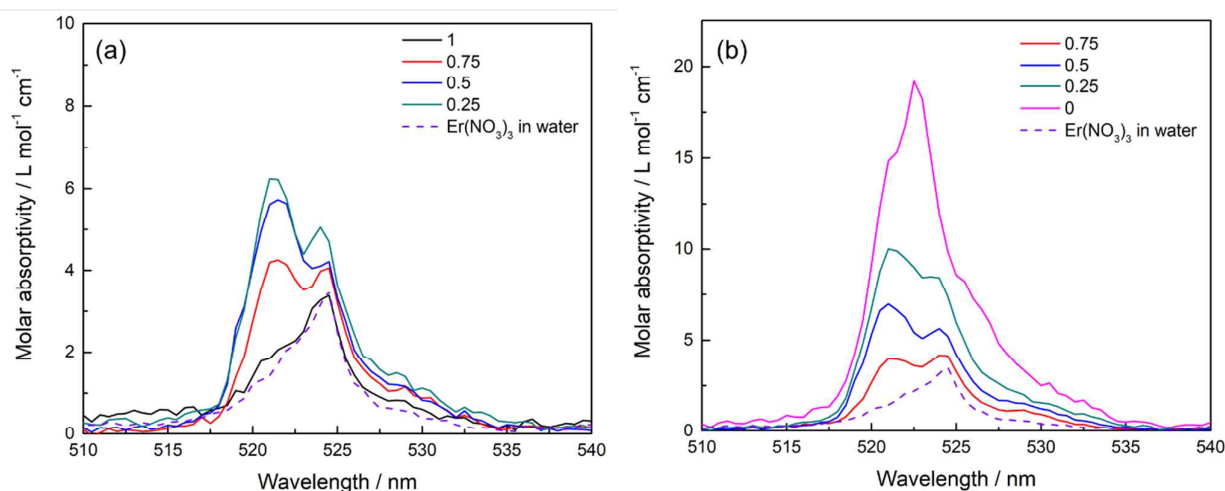


Figure 5. UV-vis absorption spectra of the organic phase after extraction using varying extractant concentration ratios with the aqueous phase including Er³⁺ in (a) 0.001 M HNO₃ and (b) 0.5 M HNO₃.

Before testing the effect of combining AOT and CMPO, the organic phases with the extracted holmium from the experiments using either AOT or CMPO individually were measured. Figure 3 shows the UV-vis spectra of the organic phase after contact with an aqueous phase of different concentration of nitric acid. The organic phase included either AOT (Fig 3. (a)) or CMPO (Fig 3. (b)). The data were collected from 430 to 560 nm to see the difference between the hypersensitive peak (450 nm) and the non-hypersensitivity peak (537 nm). Since the AOT showed higher extractability, the peak intensity of holmium should be higher for the AOT extraction. However, the intensity of the band centered at 450 nm, which correspond to the hypersensitive band, are similar for both AOT and CMPO extraction. The intensities of the band centered at 537 nm, which correspond to non-hypersensitive, are significantly lower for

environment around the extracted lanthanides. When polarizable ligands with high symmetry are used, the field gradient disappears and the magnitude of the induced $f \rightarrow f$ transition is insignificant and show low intensity. If a ligand with higher polarity bind to the lanthanide atom, the absorption intensity increases due to the effect of the electron donating ability of the ligand⁴¹.

Our earlier study suggests that AOT extracts lanthanides by forming reverse micelles which includes lanthanide ions solvated by water forming a symmetrical environment. However, CMPO extracts trivalent metal cations by the formation of lipophilic metal-CMPO-nitrate ternary species, $M(NO_3)_3(CMPO)_3$ in the organic phase^{35,42-44}. Because of this, the extractability of metal ions increase in acidic solutions but the extraction is also possible from lower acidic medium if

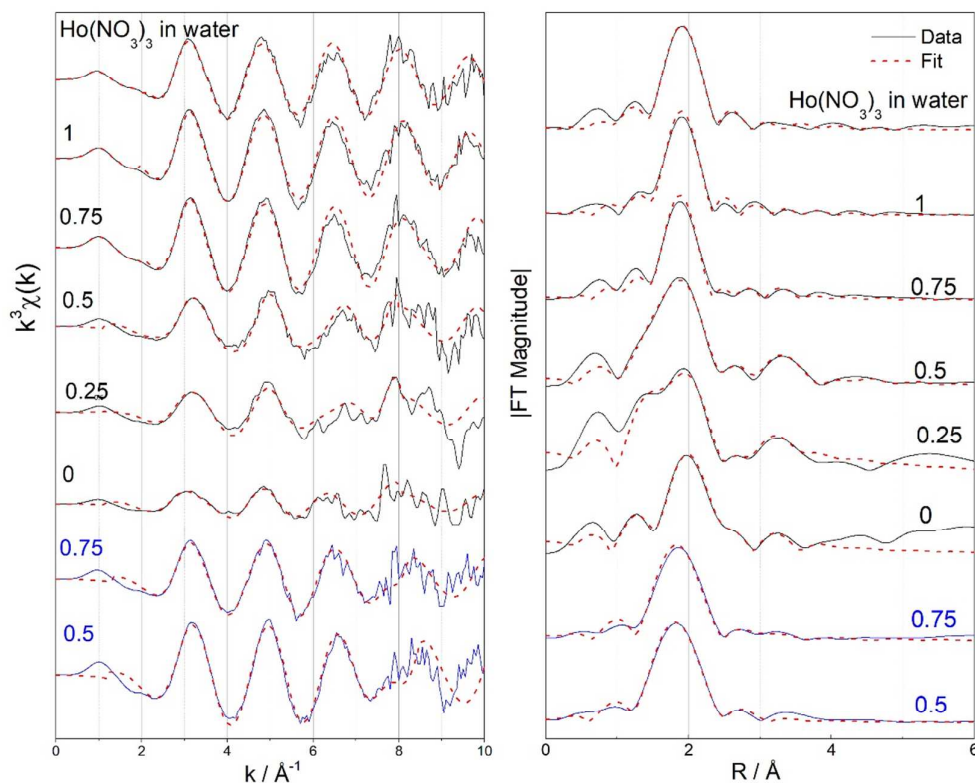
nitrate anion coexists in a sufficient concentration^{45,46}. Based on this extraction mechanism, CMPO may cause asymmetrical conditions around lanthanide ions resulting in the high absorbance of the hypersensitive band. It is worth noting that the holmium absorption in the CMPO organic phase decreases when using 5 M HNO₃ in the aqueous phase. Although high nitric acid concentration promotes Ho extraction, as mentioned above, CMPO may also extract nitric acid which cause the amount of CMPO available to complex metal ions to decrease^{36,37}. This is likely the reason for the low absorption of Ho in the organic phase when contacting with 5 M HNO₃, see figure 3b.

The UV-Vis spectrum of the organic phase including extracted Ho³⁺ or Er³⁺ with AOT-CMPO mixed system was measured for all different AOT ratios except for the case of CMPO itself (AOT ratio of 0) at low acid concentration (0.001 M) and AOT itself (AOT ratio of 1) at high acid concentration (0.5 M HNO₃) due to the low concentration of metal in the organic phase for those two conditions. Figure 4 shows the spectra from the organic phase, containing different AOT and CMPO concentration ratios, after contact with an aqueous phase containing 0.01 M holmium nitrate. Only the hypersensitive band is shown in Figure 4. The difference between Fig 4. (a) and (b) is the acid concentration in the aqueous phase. For low acid concentration, the spectrum of the holmium nitrate dissolved in the aqueous phase and the spectrum of holmium extracted with only AOT shows the same band shape structure. However, once the AOT ratio decrease, the intensity of the peak around 450 nm increase and split into three peaks. For the AOT ratios of 0.5 and 0.25, the band showed similar shape and intensity. This suggest that AOT

itself extract holmium from the aqueous phase as a hydrated form into the water core of the reverse micelle and not as a complex with AOT. As the AOT ratio decrease, CMPO substitutes the water and forms complexes with holmium ion. For the organic phase with high AOT ratio (0.75) contacted with high acid concentration, the band shape is similar to the low acid concentration band shape. However, once AOT ratio decrease to 0.25, the band shape turns into the double peak band similar to Ho extracted with CMPO only. Furthermore, the intensity of the peak in the organic phase containing high CMPO concentration is twice that of the peak for Ho extracted with AOT itself which can be explained by the symmetry of the lanthanide ion, as discussed above.

Similar to the holmium studies, erbium was also tested with different concentration ratio of AOT and CMPO contacted with aqueous solutions of different acid concentration. Erbium exhibits a hypersensitive absorption band between 520 to 525 nm owing to the ⁴I_{15/2} → ²H_{11/2} transition. Figure 5 shows the UV spectra of the organic phase following extraction with different AOT ratio at two different HNO₃ concentrations. When erbium was extracted with AOT by itself, the band shape is identical to the erbium nitrate aqueous solution (black and dashed purple lines in Fig. 5(a) for AOT extraction and Erbium in aqueous phase, respectively). This indicate that AOT itself extract erbium in a symmetric hydrated form, directly comparable to the case of Ho extraction by AOT.

However, when the AOT ratio is 0.75 or less, a second peak centered at 521 nm appeared, effectively forming a double peak. The intensity of the lower wavelength peak (at 521 nm) increase with decreasing AOT ratio. For extraction of erbium from high acidic aqueous solution using only CMPO, the band



shape and intensity of erbium is significantly changed (Fig 5 (b) AOT ratio = 0) and show a peak centered at 523 nm with a small shoulder at 521 nm. This indicates that the complex formed between CMPO and erbium nitrate cause an asymmetric condition around Er^{3+} .

As mentioned above, the significant band shape change observed in the UV-Vis data with different AOT ratio can be explained by changes in the surrounding environment of lanthanide such as different coordinating molecules or change in coordination number. Finally, bound hydrated water ions may affect the spectral change^{18,40}.

XAFS

The $k^3\chi(k)$ EXAFS data and the corresponding Fourier transform (FT) data for the extracted Ho with different AOT ratio from low and high acid concentration of the aqueous phase are shown in Fig. 6. For the data for higher acid concentration, only AOT ratios of 0.75 and 0.5 are included in this study due to the low concentration of extracted holmium in the solution. For AOT itself (AOT ratio = 1), the k-space and R-space data looks similar to holmium nitrate dissolved in water. For CMPO itself (AOT ratio = 0), the data showed different features compared to the organic phase using AOT which showed a wider and deeper oscillation peak around 2 \AA^{-1} and a double peak signal at around 4 \AA^{-1} . As the CMPO concentration in the mixture increase, the features observed using CMPO by itself gradually appeared. For higher AOT ratio, the FT data of the organic phase shows an intense peak at 1.9-2.0 \AA (before phase shift correction) attributed to the nearest oxygen neighbors. The peak around 2.5 \AA for AOT itself and 75% of AOT mixture is more likely a back-scattering oscillation feature rather than second coordination feature due to multiple small peaks. However, for lower AOT ratio, two peaks of physical significance appear. The additional peak located at 3.3~3.45 \AA (before phase shift) is attributed to the distant P atoms from the second coordination shell.

For high acid aqueous concentration (Figure 6 bottom), the k-space data, plotted as k^3 , show similar features at lower wavenumber for the two samples, but have different features at higher wavenumber. For an AOT ratio of 0.75, the low k-space range showed similar properties with the organic phase extracted with AOT itself. However, for an AOT ratio of 0.5 a wider, double peak, feature was observed around 2 \AA^{-1} which is similar to the organic phase at low acid with higher amount of CMPO.

Figure 7 shows the result of the k^3 weighted EXAFS data and corresponding Fourier transform data of the organic phase after contact with the aqueous phase containing 0.01 M Er in 0.001 M HNO_3 . The organic phase with only CMPO was not

analyzed due to its low extractability of erbium using low acid concentration. For the k-space data, two major changes are observed as the AOT ratio decrease. The oscillation around 4 \AA^{-1} shifted slightly to higher wavenumber and the oscillation around 6 \AA^{-1} gets wider as the AOT ratio decrease. The FT Er data shows an intense peak at 1.9-2.0 \AA (before phase shift correction) attributed to the nearest O neighbors. For lower AOT ratio, an additional peak located at 3.3~3.45 \AA (before phase shift) is observed, attributed to the distant P atoms from the second coordination shell.

The associated linear least squared fitting of the EXAFS data of Ho and Er are shown in Table 1 and 2. The result of the fit indicate that Ho is close to 8-coordinate with O at 2.34 \AA bond length of Ho-O for the organic phase with AOT by itself. This result is comparable to the holmium nitrate dissolved in the aqueous phase which showed similar coordination number and bond length. As the concentration of CMPO increase, the average distance of Ho-O decreased to 2.25 \AA and the coordination number is also slightly decreased. Once CMPO binds with a lanthanide, the water is replaced by an oxygen from P=O of CMPO and the distance between the lanthanide and the oxygen decrease. This behaviour was observed in previous experimental studies^{24,25,27,48} related to synergistic effect of neutral complexing agent and has also been observed in DFT simulations⁴⁷.

The erbium data showed a similar trend as the holmium EXAFS data. From the literature, the average coordination number and bond length of the erbium ion in the aqueous phase are 7.4 and 2.33 \AA , respectively⁴⁸. Comparing these numbers to our result of the organic phase contacted with the Er solution with low acid concentration showed similar bond length and coordination number. As with holmium, when the CMPO concentration increase the Er-O distance and coordination number decreased.

Table 3 shows the corresponding fitting result of the organic phase contacted with the aqueous phase including 0.5 M HNO_3 . The EXAFS fitting result can be compared with the low acid aqueous concentration data from Table 1. When the AOT ratio is 0.5 for higher acid concentration, the distance of Ho-O is shorter, and the coordination number is smaller than for the lower acid concentration case. This can be explained by higher affinity with CMPO at high acid concentration in the aqueous phase. This indicate that CMPO contribute more to the extraction of lanthanides at higher aqueous acid concentration, as would be expected.

Table 1 Ho-O EXAFS fit results for organic solutions where Ho^{3+} was extracted from an aqueous phase with 0.001 M HNO_3 . r is the interatomic distance, CN is the coordination number, σ^2 is the Debye-Waller Factor, ΔE is the energy threshold value, R-factor indicate the goodness of the fit.

| R / \AA | err | CN | err | σ^2 / \AA^2 | err | ΔE / eV | err | R-factor |
|-------------------|-----|----|-----|------------------------------|-----|-----------------|-----|----------|
|-------------------|-----|----|-----|------------------------------|-----|-----------------|-----|----------|

ARTICLE

Journal Name

| | | | | | | | | | | |
|--|------|------|----------|-----|-------|---------|----------|-------|--------|--------|
| Ho(NO ₃) ₃ dissolved in Water | Ho-O | 2.34 | 1.0E-03 | 8.3 | 0.017 | 0.00139 | 3.57E-05 | 0.369 | 0.005 | 0.0123 |
| [AOT]/[AOT+CMPO] =1 | Ho-O | 2.34 | 4.30E-05 | 7.9 | 0.004 | 0.0005 | 1.67E-05 | 0.373 | 0.0005 | 0.0146 |
| [AOT]/[AOT+CMPO] =0.75 | Ho-O | 2.35 | 2.80E-05 | 7.6 | 0.002 | 0.0007 | 8.09E-05 | 1.031 | 0.784 | 0.0130 |
| | Ho-P | 3.32 | 2.08E-02 | 0.2 | 0.301 | 0.0159 | 1.32E-02 | | | |
| [AOT]/[AOT+CMPO] =0.5 | Ho-O | 2.25 | 1.00E-05 | 7.7 | 0.002 | 0.00097 | 1.11E-06 | 0.708 | 0.024 | 0.0158 |
| | Ho-P | 3.48 | 4.32E-02 | 0.5 | 0.328 | 0.0025 | 1.12E-03 | | | |
| [AOT]/[AOT+CMPO] =0.25 | Ho-O | 2.25 | 3.54E-05 | 7.8 | 0.003 | 0.00529 | 1.39E-05 | 0.523 | 0.008 | 0.0135 |
| | Ho-P | 3.48 | 6.32E-02 | 3.0 | 0.043 | 0.00053 | 1.01E-04 | | | |
| [AOT]/[AOT+CMPO] =0 | Ho-O | 2.25 | 2.03E-04 | 7.7 | 0.006 | 0.0053 | 1.24E-05 | 0.703 | 0.007 | 0.0129 |
| | Ho-P | 3.53 | 2.12E-03 | 3.0 | 0.173 | 0.0033 | 1.24E-04 | | | |

Table 2 Er-O EXAFS fit results organic solutions where Er³⁺ was extracted from an aqueous phase with 0.001 M HNO₃. r is the interatomic distance, CN is the coordination number, σ^2 is the Debye-Waller Factor, ΔE is the energy threshold value, R-factor indicate the goodness of the fit.

| | | R / Å | err | CN | err | σ^2 / Å | err | ΔE / eV | err | R-factor |
|------------------------|------|-------|----------|-----|-------|----------------|----------|-----------------|--------|----------|
| [AOT]/[AOT+CMPO] =1 | Er-O | 2.34 | 4.30E-05 | 7.9 | 0.004 | 0.0005 | 1.67E-05 | 0.373 | 0.0005 | 0.01467 |
| [AOT]/[AOT+CMPO] =0.75 | Er-O | 2.35 | 2.80E-05 | 7.6 | 0.002 | 0.0007 | 8.09E-05 | 1.303 | 0.914 | 0.0182 |
| | Er-P | 3.24 | 0.53E-02 | 0.1 | 0.404 | 0.0109 | 2.56E-02 | | | |
| [AOT]/[AOT+CMPO] =0.5 | Er-O | 2.25 | 1.00E-05 | 7.7 | 0.002 | 0.0010 | 1.11E-06 | 0.413 | 0.012 | 0.0013 |
| | Er-P | 3.56 | 0.13E-02 | 1.0 | 0.132 | 0.0013 | 1.07E-03 | | | |
| [AOT]/[AOT+CMPO] =0.25 | Er-O | 2.25 | 3.54E-05 | 7.8 | 0.003 | 0.00529 | 1.39E-05 | 0.372 | 0.027 | 0.0112 |
| | Er-P | 3.54 | 1.28E-02 | 3.0 | 0.782 | 0.00041 | 1.01E-04 | | | |

Table 3 Ho-O EXAFS fit results for organic solutions where Ho³⁺ was extracted from an aqueous phase with 0.5 M HNO₃. r is the interatomic distance, CN is the coordination number, σ^2 is the Debye-Waller Factor, ΔE is the energy threshold value, R-factor indicate the goodness of the fit.

| | | R / Å | err | CN | err | σ^2 / Å | err | ΔE / eV | err | R-factor |
|-------------------------|------|-------|----------|-----|----------|----------------|----------|-----------------|-------|----------|
| [AOT]/[AOT+CMPO] = 0.75 | Ho-O | 2.26 | 3.15E-05 | 7.1 | 3.66E-05 | 0.006 | 2.53E-05 | 2.013 | 0.518 | 0.0106 |
| | Ho-P | 3.50 | 1.01E-03 | 1 | 3.28E-01 | 0.01843 | 1.84E-02 | | | |
| [AOT]/[AOT+CMPO] = 0.5 | Ho-O | 2.25 | 1.23E-05 | 7.3 | 0.32E-04 | 0.0023 | 3.12E-05 | 1.206 | 0.051 | 0.0109 |
| | Ho-P | 3.63 | 1.25E-02 | 3.0 | 5.00E-03 | 0.02825 | 1.72E-02 | | | |

Table 4 Parameters obtained from the XANES fitting for the organic phase including Ho³⁺

| Ho ³⁺ , 0.001M HNO ₃ | | | | | | |
|--|--------|-----|------|-----|--------|-----|
| Sample | Center | err | FWHM | err | Height | err |
| [AOT]/[AOT+CMPO] = 1 | 8073.5 | 0.1 | 6.82 | 0.1 | 3.07 | 0.2 |
| [AOT]/[AOT+CMPO] = 0.75 | 8073.5 | 0.2 | 6.95 | 0.1 | 3.07 | 0.5 |
| [AOT]/[AOT+CMPO] = 0.5 | 8073.5 | 0.1 | 6.98 | 0.1 | 3.20 | 0.2 |
| [AOT]/[AOT+CMPO] = 0.25 | 8073.5 | 0.2 | 7.01 | 0.2 | 3.36 | 0.2 |
| [AOT]/[AOT+CMPO] = 0 | 8073.3 | 0.2 | 7.12 | 0.1 | 4.14 | 0.3 |
| Ho(NO ₃) ₃ dissolved in water | 8073.5 | 0.1 | 6.09 | 0.2 | 3.68 | 0.2 |
| Ho ³⁺ , 0.5M HNO ₃ | | | | | | |
| Sample | Center | err | FWHM | err | Height | err |
| [AOT]/[AOT+CMPO] = 0.75 | 8073.5 | 0.1 | 6.34 | 0.1 | 3.62 | 0.5 |
| [AOT]/[AOT+CMPO] = 0.5 | 8073.5 | 0.1 | 7.14 | 0.2 | 3.17 | 0.2 |

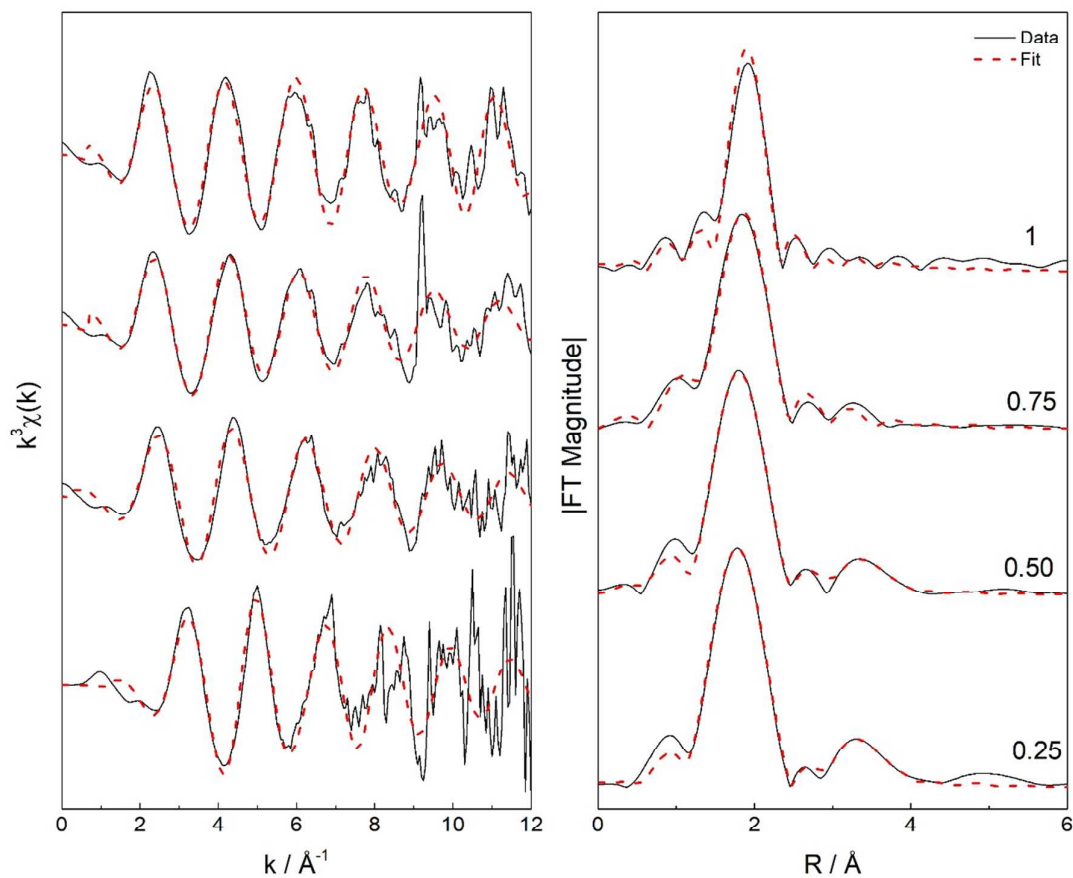


Figure 7. (Left) $k^3\chi(k)$ EXAFS data of organic phase extracting from aqueous phase containing 0.01 M Er^{3+} in 0.001 M HNO_3 with different composition of AOT and CMPO. (Right) Fourier transform data of the $k^3\chi(k)$ EXAFS (black) and the corresponding fits (red). The AOT ratio ($[\text{AOT}]/[\text{AOT}+\text{CMPO}]$) is given by each line.

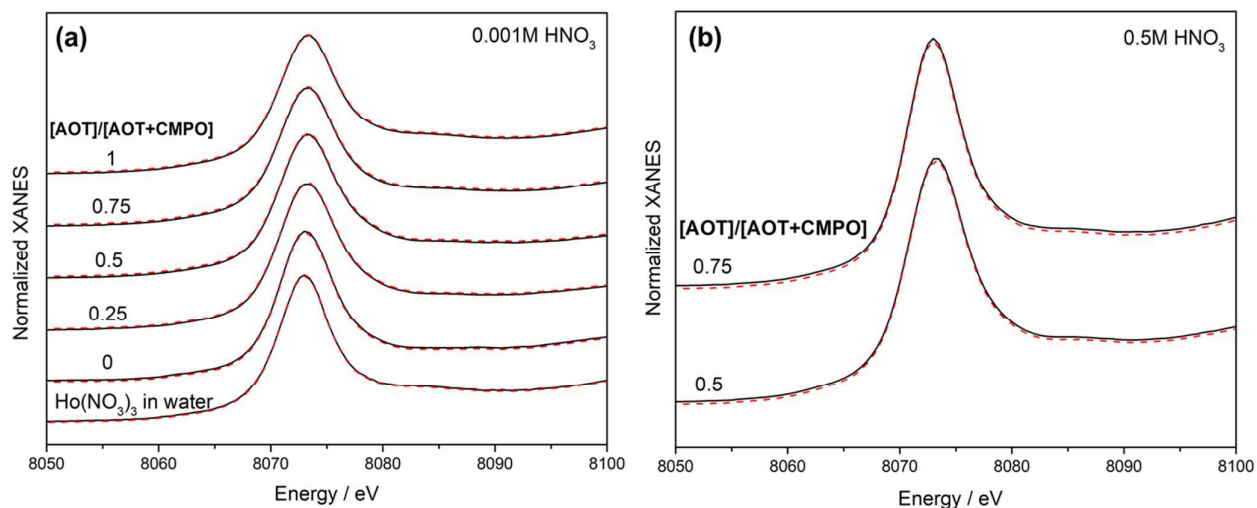


Figure 8. Normalized L-III edge XANES fitting for extracted Ho^{3+} in 0.001M HNO_3 (left) and 0.5 M HNO_3 (right) Corresponding fits are shown as red dashed lines.

The phosphorous atoms located in the second coordination sphere give a direct indication to the increased binding affinity of CMPO. It can be seen that when the acid concentration increases in the aqueous phase the corresponding coordination numbers for the P atoms increase compared to the same AOT ratio at low nitric acid concentration. Furthermore, at an AOT ratio of 0.25 or below for the low acid case, and 0.5 for high acid, there appear to be three CMPO molecules surrounding the lanthanide ion. This compares well with the stoichiometry reported previously for CMPO extraction of trivalent lanthanides and actinides from nitrate media^{35,36,49}.

Comparing the results of our EXAFS analysis in terms of bond lengths and coordination number with the previous work of Yaita et al.²³ the average bond lengths in our work are

comparable for complexation with CMPO but the coordination number of phosphorous atoms are different. In the work of Yaita et al. the Ho—O bond in the CMPO complex was found to be 2.31 Å, and the Ho—P distance was found to be 3.51 Å. Our average Ho—O and Ho—P distances are relatively similar to their work at 2.25 Å and 3.53 Å. However, we observe a coordination number of 3 for phosphorous atoms. Furthermore, Yaita et al. report on Ho—C distances for the carbonyl group while we were unable to observe this. There are some important differences in the experimental approach as well as the data analysis that may account for some of the discrepancy. First of all, the Ho—CMPO complexes in the work by Yaita et al. were prepared by mixing CMPO and holmium chloride salt in ethanol while in our work the complexes were formed during extraction of Ho, along with three nitrate ions,

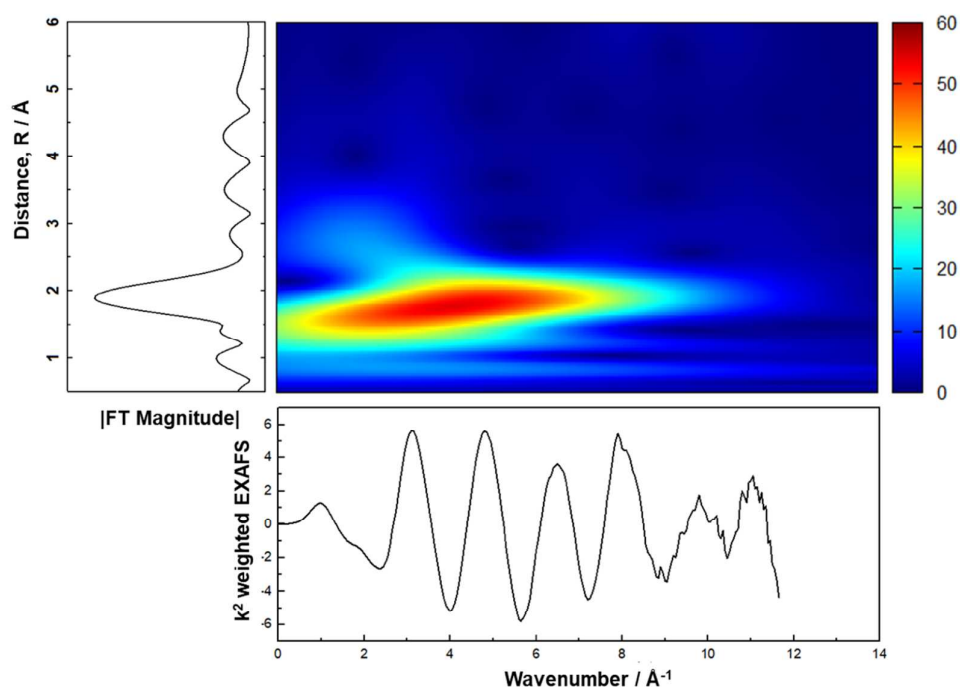


Figure 9. Overview of the wavelet transform modulus of holmium nitrate in the aqueous phase analyzed at Ho L-III edge; k-space spectrum (bottom panel), magnitude of its Fourier transform (left panel) and its Morlet wavelet transform (central panel).

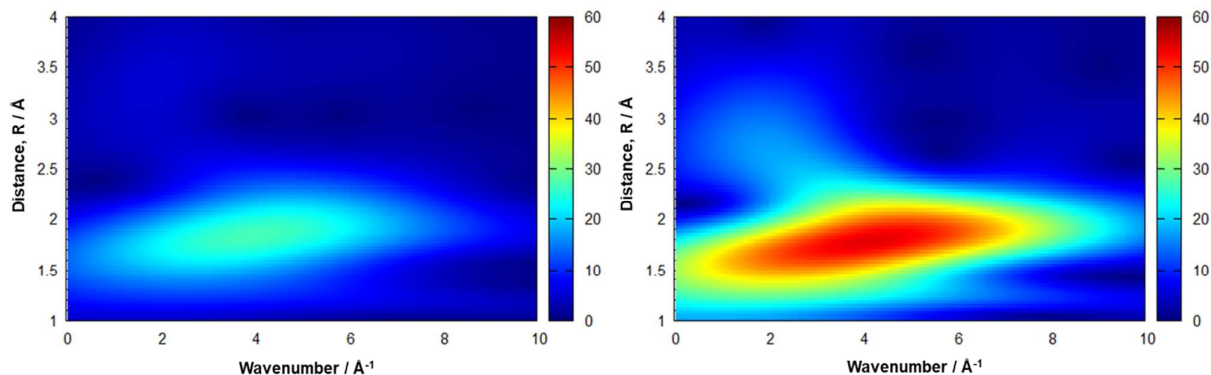


Figure 10. Wavelet transform modulus for (a) $\text{Ho}(\text{NO}_3)_3 \cdot 5\text{H}_2\text{O}$, solid (b) $\text{Ho}(\text{NO}_3)_3$ dissolved in water.

by CMPO in heptane. The concentration of metal ion, while not stated in the work by Yaita et al. may be higher than what we obtained in our work, providing better contrast for their EXAFS measurements. Second, in their work the coordination number of oxygen from water molecules, P=O and C=O groups were determined from NMR experiments and fixed in their EXAFS analysis at 4, 2, and 2, respectively. In our work, these numbers were not predetermined and were allowed to vary in the fit. Due to low contrast of our experimental data no attempt was made to separate the Ho-O oscillations between the different oxygens that should be present around the metal ion. Furthermore, the number of P-atoms at the further distance was fixed at 2 in the work of Yaita et al. while this number was again allowed to vary in our work. Finally, due to the low contrast, no attempts were made to fit a Ho—C interaction for our EXAFS data. As mentioned above, the coordination number of P atoms observed at the highest concentration of CMPO agree well with previous extraction work providing some confidence in our EXAFS fit³⁵.

Figure 7 shows the analysis of the Ho XANES, which provides further insight into the oxygen coordination environment surrounding the Ho center. The intense wide line of the normalized L-III edge XANES are characteristic of dipole-allowed electronic transitions from 2p to 5d for trivalent lanthanides⁵⁰, and their general appearance suggest that the Ho³⁺ coordination environments are similar with different ratio of AOT in AOT-CMPO mixed system. Quantitative details were extracted from the XANES spectra by using the curve fitting in Table 4. The full widths at half maximum (FWHM) increased with decreasing AOT ratio which is attributed to the change in

the coordination environment about the Ho center. This trend is caused by decreasing coordination number which correspond with the EXAFS fitting result.

To further understand the EXAFS signal for the system, wavelet transform analysis was performed for each sample. Figure 9 shows the overview of the wavelet transform of holmium nitrate in the aqueous phase. Traditional EXAFS analysis need two separated k-space and R-space graphs to qualify or quantify the data, but by combining two separate data into one contour graph, the difference caused from multi-scattering can be easily visualized. Wavelet transform contour plots were generated by decomposing the k-space and R-space (uncorrected for phase shift) signals. As a result, the wavelet transform provides detailed information on the local structure which may be difficult to identify with two separate graphs. Also, for Fourier transform, it is hard to separate different backscattering atoms in higher coordination shells present at similar bonding distance from the central lanthanide atom. Wavelet transform facilitates the identification of the backscattering atom and allow to filter out the experimental noise and can show the disorder of the structure. The color intensity is proportional to the modulus that correspond to the EXAFS amplitude term^{30,31,51}.

Figure 9 shows the spectrum of holmium nitrate dissolved in an aqueous phase. The major colored area shows the contribution from the Ho-O coordination shell. The location of the highest intensity for Ho-O in k-space were $\sim 4.5 \text{ \AA}^{-1}$ and showed longer length contribution (between 2-3 \AA in R-space). This higher length contribution is possibly coming from the Ho-O-N contribution of the nitrate since the Ho-N showed very

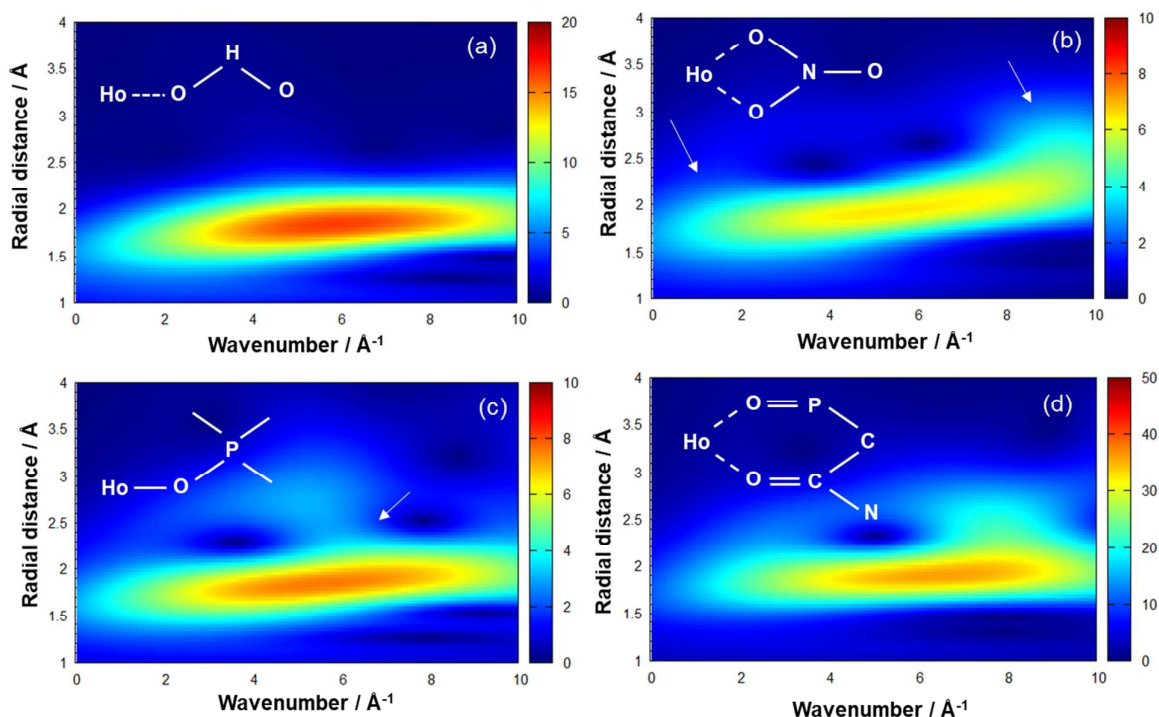


Figure 11. Simulated WT EXAFS model for Ho-O from different second backscattering atoms. (a) water, (b) nitrate, (c) monodentate binding of one phosphate and (d) a bidentate complexation of C=O and P=O from CMPO with Holmium. Each model includes Ho-O, Ho-P single scattering (for (c) and (d)) and double scattering of Ho-O-H (a) or Ho-O-N (b) or Ho-O-P (c) and Ho-O-C (d). Note that the contour density scale is different for each graph.

weak intensity at 2.3 \AA in R-space and strong oscillation occurred between 2 and 4 \AA^{-1} in k-space. Because of the different backscattering atom from the higher coordination shell, the Ho-O scattering from each nitrate, P=O, and water showed different oscillation feature in k-space causing the different R space feature of Ho-O. This can be easily visualized through wavelet transform by analyzing the deformation of the Ho-O feature. The highest intensity of this Ho-O source from Ho are different (i.e. N from the nitrate or P from the CMPO P=O bond), the backscattering from the multiple scattering amplitude and phase changed with the higher coordination shell due to its element specific properties. Figure 11 is the simulated WT transform of Ho-O single scattering path with additional multiple-scattering path from different oxygen sources such as nitrate, water and phosphate. Ho-O from water (Fig. 11 (a)) shows a horizontally wide elliptical shape without any distortion over 1.2-2 \AA radial distance and showed high intensity at the center of the shape. However, once the

hypothetical structures were simulated as references. The use of theoretical standards has become the preferred XAFS analysis and can accurately model multiple-scattering contribution as well as single scattering using reliable algorithms such as FEFF⁵². If the Ho-O distance changed, the scattering path is shifted slightly but scattering oscillation will be the same in k-space. However, if the connected oxygen from the multiple scattering amplitude and phase changed with the higher coordination shell due to its element specific properties. Figure 11 is the simulated WT transform of Ho-O single scattering path with additional multiple-scattering path from different oxygen sources such as nitrate, water and phosphate. Ho-O from water (Fig. 11 (a)) shows a horizontally wide elliptical shape without any distortion over 1.2-2 \AA radial distance and showed high intensity at the center of the shape. However, once the

Before examining the data from the extraction experiments, WT EXAFS modules for each possible Ho-O from

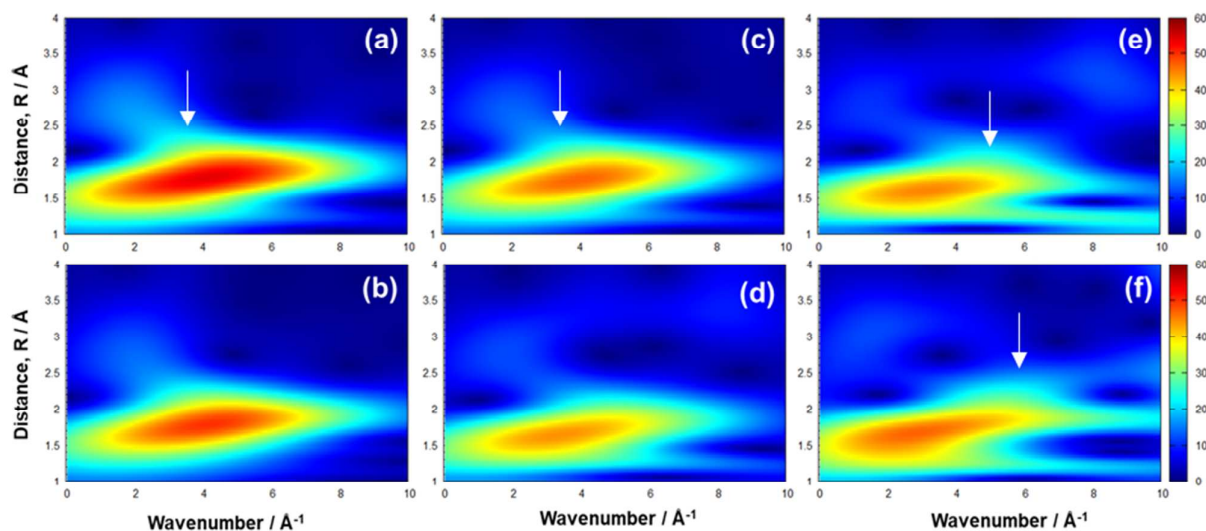


Figure 12. Wavelet transform modulus for (a) $\text{Ho}(\text{NO}_3)_3$ dissolved in water, (b) $[\text{AOT}]/([\text{AOT}]+[\text{CMPO}]) = 1$, (c) $[\text{AOT}]/([\text{AOT}]+[\text{CMPO}]) = 0.75$, (d) $[\text{AOT}]/([\text{AOT}]+[\text{CMPO}]) = 0.5$, (e) $[\text{AOT}]/([\text{AOT}]+[\text{CMPO}]) = 0.25$, and (f) $[\text{AOT}]/([\text{AOT}]+[\text{CMPO}]) = 0$ extracted with low acid concentration in the aqueous phase, plotted as a function of k (\AA^{-1}) on the x-axis and R (\AA) on the y-axis in the range of 1 to 4 \AA .

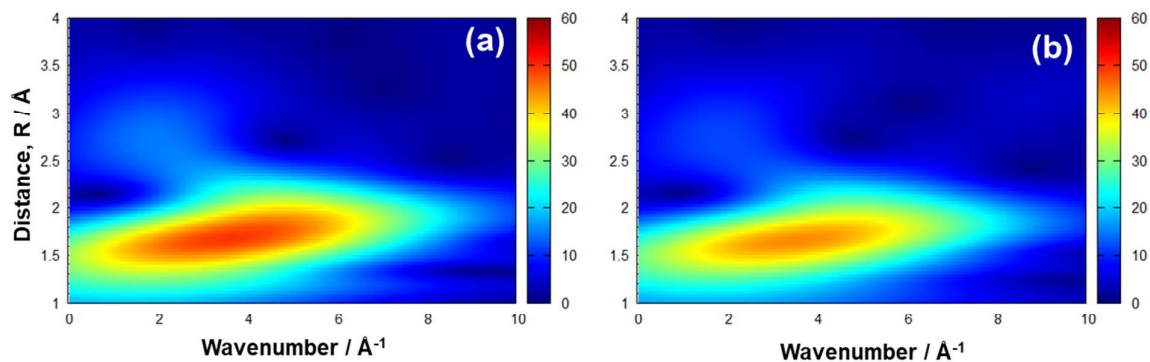


Figure 13. Wavelet transform modulus for (a) $[\text{AOT}]/([\text{AOT}]+[\text{CMPO}]) = 0.75$, (b) $[\text{AOT}]/([\text{AOT}]+[\text{CMPO}]) = 0.5$ contacted with high acid concentration in the aqueous phase, plotted as a function of k (\AA^{-1}) on the x-axis and R (\AA) on the y-axis in the range of 1 to 4 \AA .

backscattering atom from higher coordination shell is changed into N, C or P the structure is not same anymore. When the backscattering atom is the nitrogen from the nitrate, the vague low intensity increased at lower wavenumber and higher radial distance (white arrow at Fig 11. (b)) and the center density decreased. For the case when P is the backscattering atom, two different scattering models (monodentate binding of one phosphate and bidentate binding with C=P and P=O from CMPO with holmium) were visualized in Figure 11 (c) and (d). It is noteworthy that a wide low intensity circle area is observed between 4-6 Å⁻¹ and 2-3 Å radial distance for monodentate structure while the bidentate oxygen bond from CMPO showed high intensity area at 6-9 Å⁻¹ (2-3 Å radial distance).

Based on these reference spectra, the WT EXAFS data of the organic phase can be examined. Figure 12 show the organic phase contacted with the low acid aqueous phase. After holmium was extracted with the AOT itself, the shape and location are similar to the aqueous holmium nitrate sample, but the intensity decreased due to the difference in solvent beyond the hydration shell. However, the intensity of the Ho-O from the water decreased as the AOT ratio decrease, owing to the loss of water in the reverse micelle, confirmed by KF titration. It is interesting to note that the intensity at the higher wavenumber (5-6 Å⁻¹) from second coordination shell increases at lower AOT ratio (Fig. 12 (e), (f) white arrow). This can be explained by formation of M-O-P bonds with CMPO. For AOT ratio of 0.5, the intensity of the second coordination shell (wavenumber = 2.7 Å⁻¹) show a slight shift to higher wavenumber although the bidentate mode does not appear dominant at the organic phase with 0.5 of AOT ratio. Figure 13 shows the wavelet transform EXAFS of the organic phase contacted with high acid concentration in the aqueous phase. The signal intensity from the coordination shell at $k \approx 3 \text{ \AA}^{-1}$ ($R \approx 2.3 \text{ \AA}$) is decreasing and shift to higher wavenumber compared with low acid concentration (Figure 12. (b), (c)). The shift to higher wavenumber is due to increasing binding ability of CMPO at higher acid concentration.

Conclusions

In the present work, the extractability and coordination chemistry of AOT and CMPO binary extraction system was studied. The system is known to display a cooperative effect at low concentration of each extractants, but the extractability did not increase remarkably by mixing two extractant when contacting with an aqueous phase with low acid content. The extractability increased by mixing the two extractants and using higher acid concentration. However, the highest extractability of metal was observed using AOT by itself at low (0.001 M) acid concentration.

The coordination structure of lanthanide ions in this binary extraction system was studied using UV-Vis and XAFS analysis. AOT appear to extract lanthanides through reverse micelles and the extracted lanthanide exist as a hydrated ion. CMPO bind with lanthanides to form a complex with bidentate mode with C=O and P=O and decreased the amount of the hydrated water. This difference caused a significant change of the

electron configuration observed in the hypersensitive f-f transition band of the lanthanide. However, when the same amount of AOT and CMPO were applied in the system, the spectroscopic properties showed the partially complexed properties with CMPO as a reverse micelle form resulting in stable phase and increased distribution ratio. This study suggests that CMPO prevents the formation of massive micelles in the aqueous phase by partially complexing with the trivalent metal ion in the aqueous-organic interphase and aiding in the formation of reverse micelle in the organic phase.

Acknowledgements

XAFS data were collected at the Advanced Photon Source at Argonne National Laboratory on Beamline 10BM-B, supported by the Materials Research Collaborative Access Team (MRCAT). MRCAT operations are supported by the DOE and the MRCAT member institutions. This research used resources of the Advanced Photon Source, a U.S. Department of Energy (DOE) Office of Science User Facility operated for the DOE Office of Science by Argonne National Laboratory under Contract No. DE-AC02-06CH11357. The authors wish to thank Dr. Mark Antonio at Argonne National Laboratory and Dr. Carter W. Abney for helpful conversations regarding the analysis of XAFS.

References

1. M. P. Jensen, T. Yaita and R. Chiarizia, Reverse-Micelle Formation in the Partitioning of Trivalent f-Element Cations by Biphasic Systems Containing a Tetraalkyldiglycolamide, *Langmuir*, 2007, **23**, 4765-4774.
2. R. Chiarizia, M. P. Jensen, P. G. Rickert, Z. Kolarik, M. Borkowski and P. Thiyagarajan, Extraction of Zirconium Nitrate by TBP in *n*-Octane: Influence of Cation Type on Third Phase Formation According to the "Sticky Spheres" Model, *Langmuir*, 2004, **20**, 10798-10808.
3. C. C. Müller-Goymann, Physicochemical characterization of colloidal drug delivery systems such as reverse micelles, vesicles, liquid crystals and nanoparticles for topical administration, *Eur. J. Pharm. Biopharm.*, 2004, **58**, 343-356.
4. M. J. Lawrence and G. D. Rees, Microemulsion-based media as novel drug delivery systems, *Adv. Drug Deliv. Rev.*, 2012, **64**, 175-193.
5. C. Liu, B. Zou, A. J. Rondinone and Z. J. Zhang, Reverse Micelle Synthesis and Characterization of Superparamagnetic MnFe₂O₄ Spinel Ferrite Nanocrystallites, *J. Phys. Chem. B*, 2000, **104**, 1141-1145.
6. R. Shimizu, K. Sawada, Y. Enokida and I. Yamamoto, Supercritical fluid extraction of rare earth elements from luminescent material in waste fluorescent lamps, *J. Supercrit. Fluids*, 2005, **33**, 235-241.
7. J. Eastoe and B. Warne, Nanoparticle synthesis in microemulsions, *Curr. Opin. Colloid Interface Sci.*, 1996, **1**, 800-805.
8. K. Sukadeetad, W. Nakbanpote, M. Heinrich and N. Nuengchamng, Effect of drying methods and solvent extraction on the phenolic compounds of *Gynura pseudochina* (L.) DC. leaf extracts and their anti-psoriatic property. *Ind. Crops Prod.*, 2018, **120**, 34-46.
9. E. Kashi, R. Habibpour, H. Gorzin and A. Maleki, Solvent extraction and separation of light rare earth elements (La, Pr and Nd) in the presence of lactic acid as a complexing agent by Cyanex 272 in kerosene and the effect of citric acid, acetic acid and Titriplex III as auxiliary agents, *J. Rare Earths*, 2018, **36**, 317-323.
10. A. Battsengel, A. Batnasan, A. Narankhuu, K. Haga, Y. Watanabe and A. Shibayama, Recovery of light and heavy rare earth elements from apatite ore using sulphuric acid leaching, solvent extraction and precipitation, *Hydrometallurgy*, 2018, **179**, 100-109.

11. X. Huang, J. Dong, L. Wang, Z. Feng, Q. Xue, X. Meng, Selective rare earth elements from ion-adsorption rare earth element ores by stepwise extraction with HEH(EHP) and HDEHP, *Green Chem.*, 2017, **19**, 1345-1352.
12. K. E. Goklen and T. A. Hattton, Liquid-liquid extraction of low-molecular weight proteins by selective solubilisation in reversed micelles, *Sep. Sci. Technol.*, 1987, **22**, 831-841.
13. J. Rey, S. Atak, S. Dourdain, G. Arrachart, L. Berthon and S. Pellet-Rostaing, Synergistic Extraction of Rare Earth Elements from Phosphoric Acid Medium using a Mixture of Surfactant AOT and DEHCNPB, *Solvent Extr. Ion Exch.*, 2017, **35**, 321-331.
14. H. Naganawa, H. Suzuki and S. Tachimori, Cooperative effect of carbamoylmethylene phosphine oxide on the extraction of lanthanides(III) to water-in-oil microemulsion from concentrated nitric acid medium, *Phys. Chem. Chem. Phys.*, 2000, **2**, 3247-3253.
15. H. Suzuki, H. Naganawa and S. Tachimori, Extraction of Europium(III) into W/O Microemulsion Containing Aerosol OT and a Bulky Diamide. I. Cooperative Effect, *Solvent Extr. Ion Exch.*, 2003, **21**, 527-546.
16. H. Naganawa, H. Suzuki, N. Yanase, T. Nagano and J. Noro, Reversed-Micellar Extraction of Strontium(II) from Model Solutions of Seawater, *Anal. Sci.*, 2011, **27**, 321-321.
17. D. G. Karraker, Hypersensitive transitions of hydrated Nd^{3+} , Ho^{3+} , and Er^{3+} ions, *Inorg. Chem.*, 1968, **7**, 473-479.
18. D. G. Karraker, Hypersensitive Transitions of Six-, Seven-, and Eight-Coordinate Neodymium, Holmium, and Erbium Chelates, *Inorg. Chem.*, 1967, **6**, 1863-1868.
19. B. J. Gullekson, A. T. Breshears, M. A. Brown, J. B. Essner, G. A. Baker, J. R. Walensky, A. Paulenova and A. V. Gelis, Extraction of Water and Speciation of Trivalent Lanthanides and Americium in Organophosphorus Extractants, *Inorg. Chem.*, 2016, **55**, 12675-12685.
20. D. C. Koningsberger and R. Prins, *X-ray absorption: principles, applications, techniques of EXAFS, SEXAFS, and XANES*, John Wiley and Sons, New York, NY, United States, 1988.
21. M. G. Ferrier, B. W. Stein, S. E. Bone, S. K. Cary, A. S. Ditter, S. A. Kozmior, J. S. L. Pacheco, V. Mocko and G. T. Seidler, The coordination chemistry of Cm^{III} , Am^{III} , Ac^{III} in nitrate solutions: an actinide L3-edge EXAFS study, *Chem. Sci.*, 2018, Advance Article
22. P. G. Allen, J. J. Bucher, D. K. Shuh, N. M. Edelstein and I. Craig, Coordination Chemistry of Trivalent Lanthanides and Actinide Ions in Dilute and Concentrated Chloride Solutions, *Inorg. Chem.*, 2000, **39**, 595-601.
23. T. Yaita, H. Narita, S. Suzuki, S. Tachimori, H. Shiwaku and H. Motohashi, Structural study of holmium (III) and uranium (VI) organic ligand complexes by extended X-ray absorption fine-structure spectroscopy, *J. Alloys. Comp.*, 1998, **271-273**, 184-188.
24. M. R. Antonio, D. R. McAlister, E. P. Horwitz, An europium(III) diglycolamide complex: insights into the coordination chemistry of lanthanides in solvent extraction, *Dalton Trans.*, 2015, **44**, 515-521.
25. M. A. Denecke, A. Rossberg, P. J. Panak, M. Weigl, B. Schimmelpennig and A. Geist, Characterization and Comparison of Cm(III) and Eu(III) Complexes with 2,6-Di(5,6-dipropyl-1,2,4-triazin-3-yl)pyridine Using EXAFS, TRLFS, and Quantum-Chemical Methods, *Inorg. Chem.*, 2005, **44**, 8418-8425.
26. R.J. Ellis, Acid-switched Eu(III) coordination inside reverse aggregates: Insights into a synergistic liquid-liquid extraction system, *Inorg. Chim. Acta*, 2017, **460**, 159-164.
27. M. Weigl, M. A. Denecke, P. J. Panak, A. Geist and K. Gompper, EXAFS and time-resolved laser fluorescence spectroscopy (TRLFS) investigations of the structure of Cm(III)/Eu(III) complexed with di(chlorophenyl)dithiophosphinic acid and different synergistic agents, *Dalton Trans.*, 2005, **0**, 1281-1286.
28. A. D. Braatz, M. R. Antonio, and M. Nilsson, Structural study of complexes formed by acidic and neutral organophosphorous reagents, *Dalton Trans.*, 2017, **46**, 1194-1206.
29. M. Muñoz, F. Farges and P. Argoul, Continuous Cauchy wavelet transform of XAFS spectra, *Phys. Scr.*, 2005, vol **T115**, 221-222.
30. H. Funke, A. C. Scheinost and M. Chukalina, Wavelet analysis of extended x-ray absorption fine structure data, *Phys. Rev. B*, 2005, **71**, 094110.
31. L. Shao, X. Lin and X. Shao, A wavelet transform and its application to spectroscopic analysis, *Appl. Spectrosc. Rev.*, 2002, **37**, 429-450.
32. A. J. Kropf, J. Katsoudas, S. Chattopadhyay, T. Shibata, E. A. Lang, V. N. Zryyanov, B. Ravel, K. Mclvor, K. M. Kemner, K. G. Scheckel, S. R. Bare, J. Terry, S. D. Kelly, B. A. Bunker and C. U. Segre, The New MRCAT (Sector 10) Bending Magnet Beamline at the Advanced Photon Source, *AIP Conference Proceedings*, 2010, **1234**, 299-302.
33. B. Ravel and M. Newville, Athena, Artemis, Hephaestus: Data Analysis for X-Ray Absorption Spectroscopy Using IFFEFIT, *J. Synchrotron Radiat.*, 2005, **12**, 537-541.
34. J. Timoshenko, A. Kuzmin and J. Purans, EXAFS study of hydrogen intercalation into ReO_3 using the evolutionary algorithm, *J. Phys.: Condens. Matter*, 2014, **26**, 055401.
35. E. P. Horwitz, D. C. Kalina, H. Diamond, G. F. Vandegrift and W. W. Schulz, The TRUEX Process - A Process for the Extraction of the Transuranic Elements from Nitric Acid in Wastes Utilizing Modified PUREX Solvent, *Solvent Extr. Ion Exch.*, 2007, **3**, 75-109.
36. D. J. Chaiko, D. R. Fredrickson, L. Reichley-yinger and G. F. Vandegrift, Thermodynamic Modeling of Chemical Equilibria in Metal Extraction, *Sep. Sci. Technol.*, 1988, **23**, 1435-1451.
37. B. R. Spencer, R. M. Counce and B.Z. Egan, Extraction of Nitric Acid from Aqueous Media with $\text{O}(\text{D})(\text{IB})\text{CMPO}-n$ -Dodecane, *AIChE Journal*, 1997, **43**, 555-564.
38. B. Tamamushi, N. Watanabe, The formation of molecular aggregation structures in ternary system: Aerosol OT/water/iso-octane, *Colloid Polym. Sci.*, 1980, **258**, 174-178.
39. J. Moon and M. Nilsson, Investigation on the properties of micelle and reverse micelle in water/AOT/Heptane system. In *Nuclear Energy Innovation to the Carbon-Free World*. Proceedings of GLOBAL 2017, International Nuclear fuel cycle conference, Seoul, South Korea, 2017.
40. B. R. Judd, Hypersensitive Transitions in Rare-Earth Ions, *J. Chem. Phys.*, 1966, **44**, 839-840.
41. A. Chrissanthopoulos and G. N. Papatheodorou, Temperature dependence of the $f \leftarrow f$ hypersensitive transitions of Ho^{3+} and Nd^{3+} in molten salt solvents and the structure of the $\text{LaCl}_3\text{-KCl}$ melts, *J. Molec. Struct.*, 2006, **782**, 130-142.
42. E. Philip Horwitz, H. Diamond, K. A. Martin and R. Chiarizia, Extraction of Americium(III) from Chloride Media by Octyl(phenyl)-N,N-diisobutylcarbamoylmethylphosphine oxide, *Solvent Extr. Ion Exch.*, 1987, **5**, 419-446.
43. T. Fujii, K. Aoki and H. Yamana, Effect of Nitric Acid Distribution on Extraction Behavior of Trivalent F-Elements in a TRUEX System, *Solvent Extr. Ion Exch.*, 2006, **24**, 347-357.
44. K. L. Nash, Separation Chemistry for Lanthanides and Trivalent Actinides, in *Handbook on the Physics and Chemistry of Rare Earths*, ed. K. A. Gschneidner Jr., L. Eyring, G. R. Choppin, and G. H. Lander, North-Holland, Amsterdam, The Netherlands, 1994, vol. 18, pp. 197-238.
45. Y. Koma, M. Watanabe, S. Nemoto and Y. Tanaka, Trivalent f-Element Intra group Separation by Solvent Extraction with CMPO-complexant System, *J. Nucl. Sci. Technol.*, 1998, **35**, 130-136.
46. L. H. Delmau, N. Simon, M.-J. Schwing-Weill, F. Arnaud-Neu, J.-F. Dozol, S. Eymard, B. Tournois, C. Gruttner, C. Musigmann, A. Tunayar, and V. Bohmer, Extraction of trivalent lanthanides and actinides by "CMPO-like" calixarenes, *Sep. Sci. Technol.*, 1999, **34**, 863-876.
47. C. Z. Wang, W. Q. Shi, J. H. Lan, Y. L. Zhao, Y. Z. Wei and Z. F. Chai, Complexation Behavior of Eu(III) and Am(III) with CMPO and Ph2CMPO Ligands: Insights from Density Functional Theory. *Inorg. Chem.*, 2013, **52**, 10904-10911.
48. M. K. Bera, G. Luo, M. L. Schlossman, L. Soderholm, S. Lee and M. R. Antonio, Erbium(III) Coordination at the Surface of an Aqueous Electrolyte, *J. Phys. Chem. B*, 2015, **119**, 8734-8745.
49. P. Tkac, G. F. Vandegrift, G. J. Lumetta and A. V. Gelis, Study of the Interaction between HDEHP and CMPO and Its Effect on the Extraction of Selected Lanthanides, *Ind. Eng. Chem. Res.*, 2012, **51**, 10433-10444.
50. J. Röhrler, X-Ray Absorption and Emission Spectra, in *Handbook on the Physics and Chemistry of Rare Earths*, ed. K. A. Gschneidner Jr., L. Eyring and S. Hüfner, North-Holland, Amsterdam, The Netherlands, 1987, vol. 10, pp. 453-545.
51. H. Fei, J. Dong, M. J. Arellano-Jiménez, G. Ye, N. Dong Kim, E. L. G. Samuel, Z. Peng, Z. Zhu, F. Qin, J. Bao, M. J. Yacaman, P. M. Ajayan, D. Chen and J. M. Tour, Atomic cobalt on nitrogen-doped graphene for hydrogen generation, *Nat. Commun.*, 2015, **6**, 8668.
52. J. J. Rehr, J. J. Kas, M. P. Prange, A. P. Sorini, Y. Takimoto and F. Vila, Ab initio theory and calculations of X-ray spectra, *C. R. Physique*, 2009, **10**, 548-559.

